High-Temperature Material Lattice Combining Low Thermal Expansion, High Stiffness and Strength

by

Pamela L. Fetchko

A dissertation proposal submitted in partial fulfillment of the requirements for the degree of Master of Science
(College of Engineering – Department of Materials Science and Engineering)
in the University of Michigan
2008

Report Documentation Page

Form Approved
OMB No. 0704-0188

1. REPORT DATE	2. REPORT TYPE	3. DATES COVERED
01 FEB 2009	**N/A**	**-**

4. TITLE AND SUBTITLE	5a. CONTRACT NUMBER
High-Temperature Material Lattice Combining Low Thermal Expansion, High Stiffness and Strength	5b. GRANT NUMBER
	5c. PROGRAM ELEMENT NUMBER
6. AUTHOR(S)	5d. PROJECT NUMBER
	5e. TASK NUMBER
	5f. WORK UNIT NUMBER
7. PERFORMING ORGANIZATION NAME(S) AND ADDRESS(ES) **University of Michigan**	8. PERFORMING ORGANIZATION REPORT NUMBER
9. SPONSORING/MONITORING AGENCY NAME(S) AND ADDRESS(ES) **AFIT/ENEL BLDG 16 Rm120 Wright-Patterson AFB, OH 45433-7221**	10. SPONSOR/MONITOR'S ACRONYM(S)
	11. SPONSOR/MONITOR'S REPORT NUMBER(S) **CI09-0040**

12. DISTRIBUTION/AVAILABILITY STATEMENT
Approved for public release, distribution unlimited

13. SUPPLEMENTARY NOTES
The original document contains color images.

14. ABSTRACT

15. SUBJECT TERMS

16. SECURITY CLASSIFICATION OF:			17. LIMITATION OF ABSTRACT	18. NUMBER OF PAGES	19a. NAME OF RESPONSIBLE PERSON
a. REPORT	b. ABSTRACT	c. THIS PAGE			
unclassified	**unclassified**	**unclassified**	**UU**	**44**	

Standard Form 298 (Rev. 8-98)
Prescribed by ANSI Std Z39-18

The views expressed in this article are those of the author and do not reflect the official policy or position of the United States Air Force, Department of Defense, or the U.S. Government.

Abstract

Low or near zero thermal expansion is a desirable property for structures undergoing high heat fluxes and thermal stresses. A number of lattice concepts have been investigated to solve this issue. Unfortunately they do not display high stiffness and strength, are too complicated to allow for ease of fabrication, or are not proven at high enough temperatures from practical use on extreme temperature environments. A bi-material lattice that combines low or near zero thermal expansion with high stiffness over a wide temperature range has been introduced and discussed in previous research. This concept was effectively modeled and tested using an aluminum alloy, 7075-T6, and a titanium alloy, Ti-6Al-4V. The main objective of this research is to prove this bi-material lattice concept can be applied to higher temperature combinations of material capable of 1000^{o}C while still maintaining high strength and stiffness. Criteria for materials selection are presented. Three configuration concepts are analyzed via finite element calculations. Results show that the bi-material lattice can be used with high temperature materials up to 1000^{o}C but some adjustments in topology are required to achieve that temperature in a Ni – Nb metallic lattice.

Table of Contents

List of Figures……..5
List of Tables……...6
1. Introduction……7
2. Design Analysis……...10
   2.1. Topology Concept……10
   2.2. Materials Selection……...……12
   2.3. Modeling/Simulation……15
   2.4. Cell Geometry...……18
3. Results……..18
   3.1. Dove-tail configuration…….18
   3.2. Keyhole configuration……..19
   3.3. Rounded dove-tail configuration……..21
4. Conclusions……..23
5. Future Work…….24
6. References……....25
7. Figures……..27
8. Appendix A……..43

List of Figures

Figure 1: Curved rib diagram similar to one used by Lakes……..….27
Figure 2: Lakes lattice for thermal expansion via lateral bending displacement…….…..27
Figure 3: Sigmund & Torquato's zero expansion lattice created by topology optimization methods…….….27
Figure 4: Steeves *et al.* topology concept and calculations……...28
Figure 5: Schematic illustration of the triangular zero-thermal expansion lattice concept……...28
Figure 6: Pin-jointed lattice used in the study by Steeves and co-workers……...29
Figure 7: Coefficient of thermal expansion vs. temperature comparison of high temperature materials…….29
Figure 8: Specific Strength vs. Temperature comparison among several alloy classes……30
Figure 9: Comparison chart of nickel-cobalt alloys showing yield strength vs temperature……30
Figure 10: Comparison chart of nickel-cobalt alloys showing coefficient of thermal expansion vs. temperature……...……31
Figure 11: Comparison chart of Haynes 188 and Wah-Chang C-103 showing yield strength vs. temperature……31
Figure 12: Comparison chart of Haynes 188 and Wah-Chang C-103 showing coefficient of thermal expansion vs. temperature……32
Figure 13: Binary phase diagram of nickel-niobium interdiffusion within Haynes 188……...32
Figure 14: Boundary conditions applied to the lattice model in ABAQUS simulation…..……...33
Figure 15: Stress-strain curves for Haynes 188 at 1000^{o}C……33
Figure 16: Stress-strain curve for Wah-Chang C-103 at 1000^{o}C……...…34
Figure 17: Dovetail configuration of lattice cell……34
Figure 18: Highest stress concentrations in Haynes 188……...35
Figure 19: Highest stress concentrations in Wah-Chang -103……..35
Figure 20: Mises stresses in dovetail configuration at 200^{o}C……36
Figure 21: Overall displacement, U, of dovetail configuration at 1000^{o}C……36
Figure 22: Keyhole configuration of lattice cell……37
Figure 23: Mises stresses in keyhole configuration at 300^{o}C……37
Figure 24: Overall displacement, U. of keyhole configuration at 1000^{o}C…….…38
Figure 25: Rounded dovetail configuration of lattice cell…….....38
Figure 26: Mises stresses for rounded dovetail at 1000^{o}C…….39
Figure 27: Equivalent plastic strain for rounded dovetail at 1000^{o}C…….39
Figure 28: Displacement of rounded dove configuration at 1000^{o}C…….40
Figure 29: Stress comparison of Haynes 188 for three configurations……..40
Figure 30: Stress comparison of Wah-Chang C-103 for three configurations……..41
Figure 31: Phase fraction diagram of niobium-nickel interdiffusion within Haynes 188…….42

List of Tables

Table 1: Chemical composition percentage of Wah-Chang C-103……...……13
Table 2: Chemical composition percentage of Haynes 188…….....14
Table 3. Material properties for the candidate alloys used in the lattice model……15
Table 4: Ramberg-Osgood coefficients for Haynes 188 and Wah-Chang C-103…….17
Table 5: Highest stress values for dovetail configuration……..18
Table 6: Highest stress values for keyhole configuration……..20
Table 7: Highest stress values for rounded dovetail configuration……22
Table 8: Chemical composition of comparison alloys…….……..43

1. Introduction

Structural systems that experience extreme temperature variations during service in space applications [1-3] are subject to high thermal stresses that lead to thermo-mechanical fatigue of components. As the material is heated and cooled cyclically, the expansion and contraction of the material results in thermo-mechanical stresses that can eventually lead to failure of the material and thus the structure. Hypersonic vehicles are of particular interest in this research because the high speeds at which they operate lead to high thermal loads that in turn induce high stresses. Since future hypersonic vehicles are intended to be used more than once, they will be continuously subjected to thermal cyclic loading. This constant loading and unloading can lead to thermo-mechanical fatigue if an inadequate material is used. Therefore, a low thermal coefficient is necessary to prevent the occurrence of high thermal stresses within the material as it heats up. However, high stiffness and strength are also required to support bending moments and in-plane stresses that can occur in these structures during normal service conditions. Such a combination of material properties is rarely found in a single material. For instance, metals add weight to the structure, which is a hindrance for aerospace applications, while ceramics are brittle and thus limit the amount of strain structures can handle before fracture.

Composite materials have long been studied in order to combine two or more materials with differing mechanical properties that together could achieve a desired thermal property, such as lower thermal expansion or greater stiffness. A number of researchers [4-6] have investigated manipulating the coefficient of thermal expansion of both laminate and particle-reinforced composites to attain negative and positive values that could exceed a single material's possibilities. However, zero-coefficient of thermal expansion is difficult to attain with these types of composites.

Lakes [7] investigated a two constituent composite in which each constituent had a different thermal expansion coefficient and empty space was assumed to exist within the structure. This empty space allowed the structure itself to experience higher thermal expansion coefficients than either constituent independently. Depending on the placement of each constituent in the composite, the overall thermal expansion could be either positive or negative. This concept was demonstrated using a curved rib, as shown in Figure 1. If the higher thermal expansion constituent is on the convex side an increase in temperature will cause the rib to curve further and if it was on the concave side it will tend to straighten.

Lakes proved the importance of including void space in composites in order to alter the thermal expansion of the composite beyond the rule of mixtures. He used a lattice, as shown in Figure 2, that relied on lateral bending as demonstrated in the curved rib concept. The only drawback with this configuration is that the material has low stiffness and strength since the expansion is based on the bending of its constituents.

In the Lakes' configuration, the structure would experience either positive or negative thermal expansion; Sigmund and Torquato [8-9] furthered the concept by considering a net thermal expansion of zero in the overall structure. They recognized the need for low thermal expansion materials for structures experiencing large temperature fluctuations and thus also considered the stiffness of their configurations. They used a numerical topology optimization method based on previous work by Sigmund [10-11], Guedes and Kikuchi [12], and Bensoe *et al* [13] to determine how each constituent and void spaces should be distributed. This same model was later used by Sigmund [14] to create two-dimensional and three-dimensional composite exhibiting a higher bulk modulus and a lower shear modulus than previous composite configurations. Choosing to use a three constituent composite, two phases and a void phase as in

Lakes' research, their topology for the zero thermal expansion configuration is shown in Figure 3.

Topology optimization is defined by Patel *et al* [15] as "an iterative process that determines the best arrangement of a limited volume of structural material within a given spatial domain so as to obtain optimal mechanical performance of the design concept." His paper offers a concise comparison of three different types of methods. The topology optimization method used by Sigmund and Torquato optimizes the distribution of phases in a configuration in order to achieve desirable thermoelastic properties by solving finite-element problems where material type is periodically changed within the finite elements until the appropriate overall mechanical properties are achieved. In this case, material type and density was changed within each of the finite elements in order to change the strain energies so that uniform strain energy could be achieved. While it was proven to be successful in configuring optimal structures, it was also shown that there is a tradeoff between the topology of the structure and the overall bulk modulus of the material. Since the two materials used should have differing thermal expansion but similar stiffness values, for a net thermal expansion of zero, the bulk modulus was found to be approximately 7% of the bulk modulus of the constituents. Such a low bulk modulus means that the configuration itself has a low resistance to compression and thus low overall stiffness under compression loading conditions. In addition, the structures that were generated were too complex to allow for ease of manufacturing of near net shape components.

Steeves [16] and co-workers explored a zero or low expansion lattice concept that was not only capable of high strength and stiffness but also easy to manufacture. Their approach also takes into account void spaces within a lattice to acquire the desired thermoelastic properties while still maintaining the requisite mechanical strength of the of material structure. They

accomplish this by using a stretch-dominated lattice as opposed to the bending-dominated lattice used by Lakes. Steeves' lattice concept was demonstrated using aluminum for the high thermal expansion constituent and titanium for the low thermal expansion constituent. This configuration was successfully tested up to a temperature of 300^{o}C. Since the current research utilizes the design criteria developed by Steeves *et al.*, their concepts will be discussed in detail in the topology section below. The goal of this research program is to assess the applicability of Steeves' stretch-dominated lattice for structures that experience high-temperatures reaching 1000^{o}C that use niobium for the low thermal expansion constituent and a nickel-cobalt alloy for the high thermal expansion constituent.

2. Design Analysis

2.1 Topology Concept

Steeves *et al.* [16] developed a stretch-dominated lattice [17] consisting of two constituents that make up the lattice structure. Constituent 1 has the lower coefficient of thermal expansion and makes up a continuous lattice composed of skewed polyhedra. The polyhedra that make up the continuous lattice are skewed by angle θ from an equilateral triangle, Figure 4. Constituent 2, with the higher thermal expansion coefficient, would make up a discontinuous set of polyhedra that would be contained within the continuous lattice. In addition, the lattice consisted of two types of nodes, expansion nodes that are allowed to move as the structure is heated up and lattice nodes which are points where constituent one is connected to other cells within the lattice. In this case the expansion nodes will be points of zero expansion within the lattice. Although there are different configurations that could be used to make up the desired lattice with varying degrees of filling of the interior of the lattice, a triangular unit cell was used

in Steeves' *et al.* work and thus will be used in the current research as well. A schematic diagram illustrating the above concept with constituents and expansion nodes labeled is shown in Figure 5.

In the present configuration, the thermal expansion of constituent 2 does not affect the overall expansion of the lattice and thus the net thermal expansion of the lattice is dependent on constituent 1 as long as constituent 2 expands isotropically. The length of the unit cell, L, and the skewness of the polyhedra, ϑ, within constituent 1 determine the overall geometry of the lattice. The skewness of the polyhedra, ϑ, can be calculated using the coefficient of thermal expansion of both materials used and the length of the unit cell as shown in Equation 1. This value ϑ can then be used in conjunction with L to determine the lengths of the two constituents as shown in Equations 2 and 3. Figure 4 illustrates this concept in further detail (note $\overline{\alpha}$ is the desired net thermal expansion of the lattice).

$$\frac{\overline{\alpha}}{\alpha_1} = \frac{1-\frac{1}{2}\left(\frac{\alpha_2}{\alpha_1}\right)\sin(2\vartheta)\left(\frac{1}{\sqrt{3}}+\tan\vartheta\right)}{1-\frac{1}{2}\sin(2\vartheta)\left(\frac{1}{\sqrt{3}}+\tan\vartheta\right)} \tag{1}$$

$$l_1 = \frac{L}{2}\left(1+\sqrt{3}\tan\vartheta\right) \tag{2}$$

$$l_2 = \frac{L}{2\cos\vartheta} \tag{3}$$

Like the thermal expansion properties, solely constituent 1, the continuous lattice, will determine the structural behavior of the lattice. Figure 6 shows an example of the pin-jointed lattice studied by Steeves *et al.*, where a pin allowing each constituent to move freely without being mutually constraining attached the two materials. The model structure proved that the expansion of the lattice as a whole was near zero as the calculations suggested. In addition, the

pin-jointed lattice was found to be comparable with the Gibiansky-Torquato bounds [18], which are narrower than the Rosen-Hashin and Schapery bounds [19-20], at low area fractions. This experiment allowed for the rotation and elongation of the constituents but did not take into account the rotational resistance that will be experienced when the two constituents are bonded. The joints between the two constituents are typically made by press fitting them together , which may result in a metallurgical bond between the two materials at the point of contact with high temperature excursions. As the lattice is heated constituent 2 will apply stress to the slowly expanding constituent 1. This will lead to the in-plane bending of the continuous lattice as it resists the expansion of constituent 2.

Steeves *et al.* [16] found that the uniaxial stiffness of the lattice when bonded together is dependent on the bending stiffness of the constituents. When the net thermal expansion was equal to zero, the stiffness increased as the constituents increased in thickness allowing for a constant length. This increase in stiffness can actually cause the skewness angle, ϑ, for zero-expansion to deviate from the theoretical calculations and can possibly lead to yielding due to the applied bending stresses.

2.2 Material Selection

Steeves *et al.* [16] demonstrated the afore-mentioned concept by modeling the lattice using aluminum as constituent 2 and titanium as constituent 1 at temperatures below 300^{o}C. The current research utilizes this design concept in order to apply it to higher temperatures of at least 1000^{o}C. The material property that was of primary interest for this research was the coefficient of thermal expansion. A combination of materials was needed that have varying coefficients of thermal expansion to combine to form a composite of low thermal expansion. The coefficients

of thermal expansion of some materials [21-23] used in high temperature applications are compared in Figure 7. In this chart, Haynes 188 and Wah-Chang C-103 are also plotted for comparison. This shows that individually the two have the highest coefficients of thermal expansion over the temperature range when compared to other high-temperature materials. Additionally their coefficients of thermal expansion are different enough to achieve an overall zero expansion lattice.

In order to reach a minimum temperature of 1000^{o}C, the material chosen must retain its mechanical properties at elevated temperatures. The next mechanical property of interest for this concept is elevated temperature strength. According to the specific-strength vs. temperature chart shown in Figure 8, nickel and niobium represent the logical choice as metallic candidate materials for high-temperature applications.

In particular a nickel-cobalt alloy was chosen as the candidate high coefficient of thermal expansion material while niobium was chosen for the low coefficient of thermal expansion constituent. In addition to high-temperature strength, both materials should exhibit high toughness and ductility. Niobium was chosen not only because it retains its strength at high temperatures but also because it is lightweight compared to other refractory materials and therefore an ideal candidate for aerospace applications where weight saving is a key design consideration. For this analysis, the alloy Wah-Chang C-103 (Wah-Chang, Albany, OR, USA) will be used.

Table 1: Chemical composition percentage of Wah-Chang C-103 [22]

Nb	Hf	Ti	Zr	Ta	W
87-87.6	10	0.7-1.3	0.7	0.5	0.5

A comparison of several nickel-cobalt alloys, all Haynes International alloys, was made to determine the candidate material with superior properties for the high-temperature

applications. Nickel-cobalt superalloys exhibit high strength and good creep resistance at high temperatures, and are available in thin sheet form, thus making them an ideal choice for this research. A comparison of the 0.2% yield strength vs. temperature variation is shown in Figure 9 and a comparison of the coefficient of thermal expansion vs. temperature is shown in Figure 10 for all the alloys that were considered in this work; detailed data is further provided in Appendix A. Haynes 188 (Haynes International, Kokomo, IN, USA) alloy was chosen due to its ability to maintain high yield strengths at elevated temperatures as well as a gradual decrease in the yield strength with increase in temperature. In addition to yield strength, Haynes 188 has the highest elastic modulus and coefficient of thermal expansion among the several alloys considered here. Figure 11 and Figure 12 show a comparison of Haynes 188 and Wah-Chang C-103 for both 0.2% yield strength vs. temperature and coefficient of thermal expansion vs. temperature.

Table 2: Chemical composition (wt%) of Haynes 188 [23]

Co	Ni	Cr	W	Fe	Mn	Si	C	La	B
39	22	22	14	3	1.25	0.35	0.10	0.03	0.015

A phase diagram was constructed using Pandat [24] to determine if any brittle phases will form at the lattice joints during interdiffusion between Haynes 188 and Wah-Chang C-103. As niobium replaces nickel within Haynes 188 some brittle phases will form, as shown in Figure 13. These phases are σ (which consists mainly of nickel, cobalt, chromium, and tungsten), δ (nickel, niobium, cobalt), and C14 (niobium, cobalt, nickel). At 1000^{o}C, all three brittle phases can form. While interdiffusion will be limited at this temperature, these phases could nevertheless influence the behavior of the bi-material joints.

The material properties that were used for modeling are listed in Table 3. It is important to note that the thermal expansion coefficient listed is the average over the entire temperature

range of 20°C-1000°C, to see how the thermal expansion coefficient averages vary over the temperature range see Figure 12.

Table 3. Material properties for the candidate alloys used in the lattice model

	Density	Coefficient of Thermal Expansion		Elastic Modulus		Ultimate Tensile Strength		0.2% Yield Strength	
	(g/cm^3)	T (C)	(10^{-6}/C)	T (C)	(GPa)	T (C)	(MPa)	T (C)	(MPa)
Haynes 188	8.98	25-100	11.90	20	232	20	985.0	20	470.0
		25-200	12.60	100	225	540	775.0	540	275.0
		25-300	13.20	200	217	650	755.0	650	265.0
		25-400	13.80	300	209	760	650.0	760	270.0
		25-500	14.50	400	201	870	450.0	870	250.0
		25-600	15.20	500	193	980	265.0	980	185.0
		25-700	15.80	600	184	1095	145.0	1095	88.0
		25-800	16.50	700	176				
		25-900	17.10	800	169				
		25-1000	17.90	900	161				
				1000	153				
Wah-Chang C-103	8.85	93	6.84	20-1000	90	20	420.6	20	296.5
		204	7.02			540	310.3	540	199.9
		427	7.20			650	317.2	650	186.2
		649	7.38			760	320.6	760	172.4
		871	7.56			870	310.3	870	162.0
		982	7.74			1095	186.2	1095	137.9
		1093	7.92						

2.3 Modeling/Simulation

The finite element analysis was accomplished using the ABAQUS program [25]. Using the formulas discussed in the topology section and the two materials selected above, the ratio α_2/α_1 was calculated to be 2.313 and thus the skewness θ was determined analytically to be 26.6°. Given these two parameters the length of the unit cell, L, as well as the length of the two constituent sides, l_1 and l_2, were calculated. It is important to note that the calculations for the length of constituent 2 do not take into account the width of constituent 1. For this reason, in

order to obtain the true value of l_2, twice the thickness of constituent 1 must be subtracted from the value obtained above to account for the thickness at both connection points of constituent 2 to constituent 1.

The two constituents will be bound together using a press fit connection that is modeled by constraining corresponding nodes in the two materials to have the same displacements. In the stretch-dominated lattice thus designed a two-dimensional problem was modeled. A quadratic mesh composed of approximately 1300 8-node generalized plane strain elements was used.

Due to the symmetry of the lattice, only half of the cell was modeled, see Figure 14. This was done for simplification of the boundary conditions applied. The boundary conditions that were applied consisted of a pinned point at the center of the triangle at 30^o (half of an equilateral angle) that was constrained in the x and the y so that there was no displacement at this point. Since the pinned point is the center of a unit cell, it is thus a point of zero expansion within the lattice. The boundary condition at the pinned point also eliminates rigid body displacements within the model. Furthermore, due to symmetry, displacements along the entire left side of the cell were constrained to zero in the x direction. This constraint does not inhibit the material from moving in the y-direction along the edge of the model. These boundary conditions do not inhibit elongation of either constituent in any way and allow for an accurate simulation to be run. A detailed schematic diagram of the boundary conditions is shown in Figure 14.

The material is expected to reach its yield strength during heating or cooling and thus plastic deformation and strain hardening is expected to occur. In ABAQUS the strain hardening was modeled using the Ramberg-Osgood equation (Equation 4 below) where E is the modulus of elasticity, σ is the stress, σ_o is the yield strength, ε is the strain, α is the coefficient of thermal expansion, and n is the Ramberg-Osgood coefficient.

$$E\varepsilon = \sigma + \alpha\left(\frac{|\sigma|}{\sigma_o}\right)^{n-1}\sigma \tag{4}$$

The Ramberg-Osgood equation is used to model stress-strain response in materials that undergo strain hardening past the materials yield point. The Ramberg-Osgood coefficient, n, is a constant that depends on the material being considered. In order to calculate the value of n for Haynes 188 and Wah-Chang C-103 it was assumed that in both materials the fracture strength equaled the ultimate tensile strength. Using the material data sheets provided for both materials [22-23], the percent elongation at fracture could determine the strain at fracture when using Equation 4. This constant could then be fit in over the stress range from yield strength to ultimate tensile strength to determine the strain experienced at a certain stress and thus the stress-strain curve of the material. The resulting stress-strain curves for Haynes 188 and Wah-Chang C-103 at 1000^{o}C are shown in Figures 15 and 16 respectively. It is also important to note that Haynes 188 has a higher yield strength but a lower ultimate tensile strength over the temperature range of interest.

Table 4: Ramberg-Osgood coefficients for Haynes 188 and Wah-Chang C-103

Material	Temperature (C)	Yield Strength (MPa)	Ultimate Tensile Strength (MPa)	Percent Elongation (%)	Ramberg-Osgood coefficient
Wah-Chang C-103	20	296.5	420.6	30	23.61
	540	199.9	310.3	21	24.44
	650	186.2	317.2	17	19.90
	760	172.4	320.6	18	17.31
	870	162.0	310.3	19	16.70
	1095	137.9	186.2	45	39.60
Haynes 188	20	470.0	985.0	56	15.99
	540	275.0	775.0	69	11.96
	650	265.0	755.0	73	11.86
	760	270.0	650.0	70	14.04
	870	250.0	450.0	77	21.21
	980	185.0	265.0	84	35.64
	1095	88.0	145.0	89	27.15

2.4 Cell Geometry

The original configuration that was discussed was the dovetail design used by Steeves *et al.* in their experiments. For the materials used in this research; however, it posed a problem, which will be discussed below, as higher temperatures were reached. In order to counteract this finding two additional configurations were explored, a keyhole configuration and a rounded dovetail configuration that was modified from the original dovetail. All three configurations and their results during simulation will be presented in greater detail in the results section following.

3. Results

3.1 Dovetail Configuration

The first configuration to be discussed is the dovetail configuration originally used by Steeves *et al* [15], shown in Figure 17. This configuration allowed for a tight fit between the two materials since constituent 2 expands at a faster rate than constituent 1. This configuration was tested in 100^{o}C increments from 100^{o}C up to 1100^{o}C. At each increment the highest Mises stress within each material was recorded and the results are shown in Table 5 below.

Table 5: Highest stress values for dovetail configuration

Temperature (C)	Haynes 188 (MPa)	Wah-Chang C-103 (MPa)
100	247	123
200	531	266
300	705	353
400	644	429
500	584	389
600	563	282
700	535	401
800	451	376
900	342	342
1000	252	231
1100	173	260

Based on the findings above, the ultimate tensile strength of Haynes 188 was not reached over the entire temperature range; the same did not hold true for Wah-Chang C-103. At a temperature of 400^{o}C the ultimate tensile strength is approximately 340 MPa however the stresses experienced within the niobium constituent, constituent 1, are 429 MPa (see Figures 18 - 20). The stresses were concentrated around the expansion nodes as well as the lattice joints between the niobium constituent, constituent 1, and the nickel-cobalt alloy, constituent 2. The areas experiencing the highest stress concentrations for Haynes 188 and Wah-Chang C-103 are shown in Figures 19 and 20, respectively. This indicates that at or around 400^{o}C the lattice will fail in the vicinity of one of the sharp corners of the dovetail design due to fracturing within the material. For this reason the geometry of constituent 1 must be altered to lower stress concentrations within the niobium.

It is important to note that while the stresses were exceeded, the lattice did maintain near zero expansion at the expansion nodes up to 1000^{o}C (see Figure 21). This shows that the lattice concept can be applied to any two materials with a sufficiently different CTE in order to obtain a zero-expansion lattice.

3.2 Keyhole configuration

To recap, the stresses within constituent 1, the niobium, were the limiting factor in the dovetail configuration discussed above. The areas experiencing the highest stresses were near the expansion nodes and the lattice joints. In order to alleviate stress concentrations, a rounded joint, as opposed to one with sharp angles like the dovetail, was applied (see Figure 22). This joint will be referred to as a keyhole joint. Once again the lattice cell was tested from 100^{o}C–

1100°C in 100°C increments. The Mises stresses that develop due to expansion are summarized in Table 6 below.

Table 6: Highest stress values for keyhole configuration

Temperature (C)	Haynes 188 (MPa)	Wah-Chang C-103 (MPa)
100	59	140
200	130	309
300	213	423
400	280	372
500	319	348
600	405	338
700	466	389
800	499	376
900	451	303
1000	326	326
1100	183	243

The findings for this configuration differed from the dovetail but with the same overall result. The ultimate tensile strength of Wah-Chang C-103, 355 MPa, was reached at an earlier temperature of 300°C experiencing a stress of 423 MPa (see Figure 23). Once again the highest stress concentrations were around the expansion nodes and the bi-material lattice joints. The main difference between the keyhole and the dovetail configuration is that in the case of the keyhole the ultimate tensile strength of Haynes 188 was also reached. At approximately 900°C the ultimate tensile strength of Haynes 188 is 400 MPa and the stress experienced by Haynes 188 at the lattice joint was 451 MPa. For this configuration, fracture would occur in both materials at the lattice joint and in Wah-Chang C-103 around the expansion nodes as well.

The difference in the behavior of the Haynes 188 material in the two joint configurations can be attributed to strain hardening. In the dovetail configuration the greatest stress seen within the material occurred at 300°C while in the keyhole configuration it occurred at 800°C. The material did not undergo plastic deformation until approximately 500°C, unlike the dovetail where it occurred very early on at around 200°C, and thus was not able to undergo strain

hardening in time to strengthen the material prior to the ultimate tensile strength of the material decreasing at higher temperatures. From these results, it can be determined that strain hardening is instrumental in allowing the lattice joint to survive the expansion of the material at higher temperatures. Once again it is important to note that while the material would undergo fracture, the expansion was near zero at the expansion nodes (see Figure 24).

3.3 Rounded dovetail configuration

The keyhole configuration proved that for the Haynes 188 constituent the dovetail joint is preferred as it allows for plastic deformation and thus strain rate hardening to occur at lower temperatures. The same problem continued to occur in the Wah-Chang C-103 constituent as the ultimate tensile strength was reached at lower temperatures. For this reason, the lattice geometry must be modified to reduce stresses within the Wah-Chang C-103 constituent. The expansion nodes still experienced high stresses regardless of the joint change so a dovetail configuration for the joint will be used but the sharp corners at the expansion joints will be rounded on the inside named a rounded dovetail configuration (see Figure 25). The reason for the joint only being rounded on the inside, as opposed to both sides of the expansion joint, is because while only a single cell is being modeled here a continuous lattice will be used in practical applications. A sharp angle should be made between the two legs of constituent 1 at the zero expansion points in order to mimic the connection joint between the three cells that will eventually make up a continuous lattice. Once again the lattice cell was tested from 100^{o}C–1100^{o}C in 100^{o}C increments. The stress findings are summarized in Table 7 below.

Table 7: Highest stress values for rounded dovetail configuration

Temperature (C)	Haynes 188 (MPa)	Wah-Chang C-103 (MPa)
100	254	106
200	547	228
300	713	357
400	644	322
500	583	291
600	563	282
700	534	267
800	449	300
900	351	263
1000	263	241
1100	166	222

The findings for this configuration show that the ultimate tensile strength for both materials was not reached until 1100^{o}C indicating that failure will not occur until that temperature. The contour plot shown in Figure 26 indicates the areas of high stress within each material at 1000^{o}C. These results prove that the rounded dovetail configuration was successful in inhibiting the ultimate tensile strength from being reached until much higher temperatures than the other two configurations. This occurs because the dovetail allows the Haynes 188 constituent to strain harden early on, strengthening the material prior to higher stresses being induced by the temperature increase as was shown earlier in the dovetail configuration. The Wah-Chang C-103 constituent experiences lower stresses at both joints because of the decreased stress concentrations at the edges in this configuration. This occurs because the rounded edges not only lower stress concentrations but allow the material to bend more readily as the Haynes 188 constituent pushes against the Wah-Chang C-103 constituent at the lattice joints. This effectively causes lower stresses to be experienced in both the lattice joints and the zero-expansion joints.

The plastic strains experienced by both constituents occurred at the zero-expansion joints and the lattice joints as expected (see Figure 27). These were the areas of highest stress and thus

the ones that would experience plastic deformation. As for the remaining areas of the cell no plastic deformation occurred. This was expected, as the stresses within those areas remained small throughout the temperature increase. Once again, as in the other two configurations, the displacement at the zero-expansion joints is near zero as shown in Figure 28.

Figure 29 and Figure 30 summarize the findings of all three configurations and show the highest stress values within each material; the highest stress regions within the material are indicated in the diagrams next to the plots. The highest stresses observed in the C-103 and the Haynes 188 occurred at the same location throughout the temperature range $20^{o}C$ – $1000^{o}C$ for all three configurations investigated. In the Haynes 188 peak stresses occurred in the dovetail connection. The same held true for C-103 with the addition of the expansion nodes as well.

4. Conclusions

A bi-material lattice was modeled using ABAQUS that exhibited low thermal expansion as well as high stiffness and strength. The lattice is stretch-dominated and thus the expansion is allowed through the stretching of the constituents rather than bending. This facilitated the high stiffness of the materials to be maintained.

Using a rounded dovetail configuration the stresses within both materials could be maintained below the ultimate tensile strength. This was due to strain hardening within the Haynes 188 constituent and a facilitated bending of the Wah-Chang C-103 constituent. The displacement of the expansion nodes was proven to be minimal and essentially zero for calculation purposes.

In conclusion, the bi-material lattice design composed of nickel and niobium should be suitable for thermal excursions up to 1000^{o}C, in terms of mechanical integrity and its requisite thermal and mechanical properties.

5. Future Work

Currently more simulations are underway to determine the effects of temperature cycling on the lattice model by considering the creep characteristics of the materials used. A single cell is currently being fabricated to compare and verify the model simulations performed using ABAQUS. This cell will have a topology that allows for a net thermal expansion of 4 10^{-6}/C, thus enabling the measurement of the displacements. Subsequent to the successful demonstration of the lattice model by way of the single cell test a full panel will be fabricated and tested for survivability up to 1000^{o}C. In addition, a phase fraction diagram was constructed based on the interdiffusion of niobium with nickel within the Haynes 188 alloy, Figure 31, that showed the percent fraction of brittle phases formed within the alloy actually decrease as temperature increases. It would be of interest to further look into configuring another cell composed of Haynes 188 and Wah-Chang C-103 that would be capable of temperatures of 1200^{o}C and higher to take advantage of this finding. Also of interest would be the design of low expansion structures that take advantage of the low densities and higher temperature capabilities of C/C and C/SiC composites.

6. References

1	Blankenship, C.P. and Yu, J.C. "Structures and Materials Technology for Space Station." AIAA Paper No. 88-2446
2	Rawal, S. "Metal-Matrix Composites for Space Applications." Journal of the Minerals, Metals and Materials Society 53.4 (2001): 14-17.
3	McManus, H.L. "Control of space structure thermal deformation: an overview." Proceedings of SPIE 1917:1 (1993): 545-554.
4	Kelly, A., Stearn, R.J., and McCartney, L.N. "Composite materials of controlled thermal expansion." Composites Science and Technology 66 (2006): 154-159.
5	Kelly, A., McCartney, L.N., Clegg, W.J., and Stearn, R.J. "Controlling thermal expansion to obtain negative expansivity using laminated composites." Composites Science and Technology 65 (2005): 47-59.
6	Nadeau, J.C. and Ferrari, M. "Effective thermal expansion of heterogeneous materials with application to low temperature environments." Mechanics of Materials 36 (2004): 201-214.
7	Lakes, R. "Cellular solid structures with unbounded thermal expansion." Journal of Materials Science Letters 15 (1996): 475-477.
8	Sigmund, O. and Torquato, S. "Composites with extremal thermal expansion coefficients." Appl. Phys. Lett. 69.21 (1996): 3202-3205.
9	Sigmund, O. and Torquato, S. "Design of Materials with Extreme Thermal Expansion using a Three-Phase Topology Optimization Method." J. Mech. Phys. Solids 45.6 (1997): 1037-1067.
10	Sigmund, O. "Materials with Prescribed Constitutive Parameters: An Inverse Homogenization Problem." Int. J. Solids Structures 31.17 (1994): 2313-2329.
11	Sigmund, O. "Tailoring materials with prescribed elastic properties." Mechanics Of Materials 20 (1995): 351-368.
12	Guedes, J.M. and Kikuchi, N. "Preprocessing and Postprocessing for Materials Based on the Homogenization Method with Adaptive Finite Element Methods." Computer Methods in Applied Mechanics and Engineering 83 (1990): 143-198.
13	Bendsoe, M.P., Guedes, J.M., Haber, R.B, Pedersen, P. and Taylor, J.E. "An Analytical Model to Predict Optimal Material Properties in the Context of Optimal Structural Design." J. Appl. Mech. 61 (1995): 930-937.
14	Sigmund, O. "A new class of extremal composites." J. Mech. Phys. Solids 48 (2000): 397-428.
15	Patel, N.M., Tillostson, D., Renaud, J.E, Tovar, A., and Izui, K. "Comparitive Study of Topology Optimization Techniques." AIAA Journal 46.8 (2008): 1963-1975.
16	[4]Steeves, C., dos Santos e Lucato, S.L, He, M., Antinucci, E., Huchinson, J>W., and Evans, A.G. "Concepts for structurally robust materials that combine low thermal expansion with high stiffness." J. Mech. Phys. Solids 55 (2007): 1803-1822.
17	Deshpande, V.S., Ashby, M.F, and Fleck, N.A. "Foam Topology Bending versus Stretching Dominated Architectures." Acta Materialia 49 (2001): 1035-1040.
18	Gibiansky, L.V. and Torquato, S. "Thermal Expansion of Isotropic Multiphase Composites and Polycrystals." J. Mech. Phys. Solids 45.7 (1997): 1223-1252.
19	Rosen, B.W. and Hashin, Z. "Effective Thermal Expansion Coefficients and Specific Heats of Composite Materials." Int. J. Engng. Sci. 8 (1970): 157-173.

20	Schapery, R.A. "Thermal Expansion Coefficients of Composite Materials Based on Energy Principles." Journal of Composite Materials 2.3 (1968): 380-404.
21	MatWeb: Material Property Data. www.matweb.com.
22	Wah-Chang. C-103 Data Sheet. Wah-Chang, Albany, OR, USA.
23	Haynes International. Haynes 188 Data Sheet. Haynes International, Kokomo, IN, USA.
24	CompuTherm LLC. Pandat, 7.0 ed.
25	Simulia. ABAQUS/CAE User's Manual, 6.8 ed.
26	Johnson, S. and Pollock, T. "Metallics for Actively Cooled Structures." Presented at Workshop on Materials and Structures for Hypersonics Flight, 11 July 2007.

7. Figures

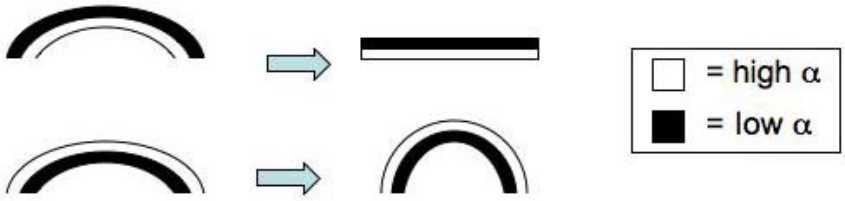

Figure 1: Curved rib diagram similar to one used by Lakes

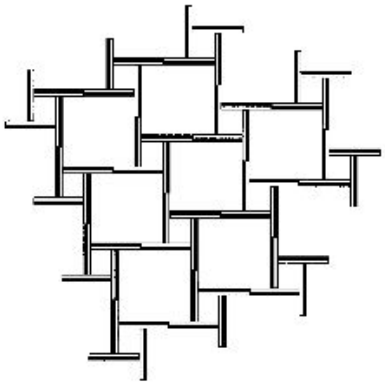

Figure 2: Lakes lattice for thermal expansion via lateral bending displacement [7]

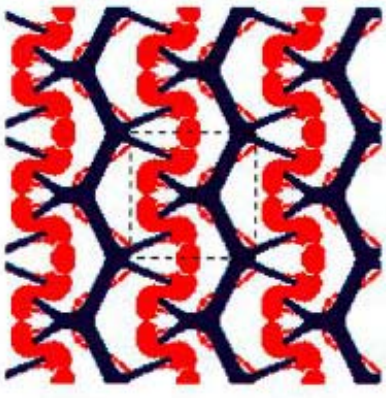

Figure 3: Sigmund & Torquato's zero expansion lattice created by topology optimization methods [8]

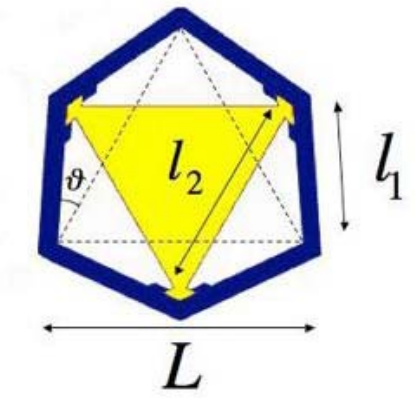

$$l_1 = \frac{L}{2}\left(1+\sqrt{3}\tan\vartheta\right)$$

$$l_2 = \frac{L}{2\cos\vartheta}$$

$$\frac{\bar{\alpha}}{\alpha_1} = \frac{1-\frac{1}{2}\left(\frac{\alpha_2}{\alpha_1}\right)\sin(2\vartheta)\left(\frac{1}{\sqrt{3}}+\tan\vartheta\right)}{1-\frac{1}{2}\sin(2\vartheta)\left(\frac{1}{\sqrt{3}}+\tan\vartheta\right)}$$

Figure 4: Steeves *et al.* topology concept and calculations [16]

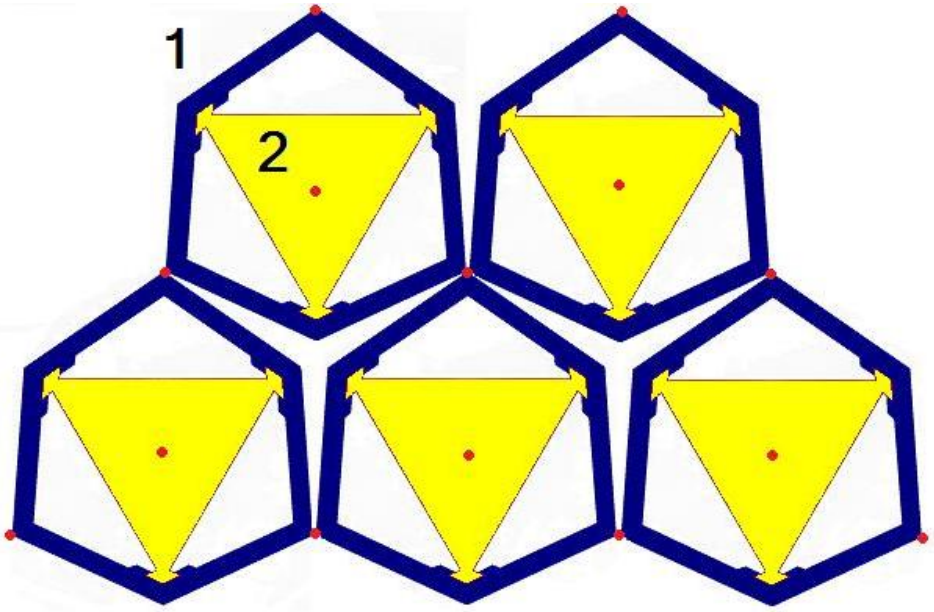

Figure 5: Schematic illustration of the triangular zero-thermal expansion lattice concept

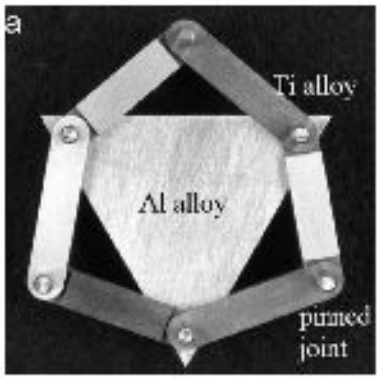

Figure 6: Pin-jointed lattice used in the study by Steeves and co-workers [16]

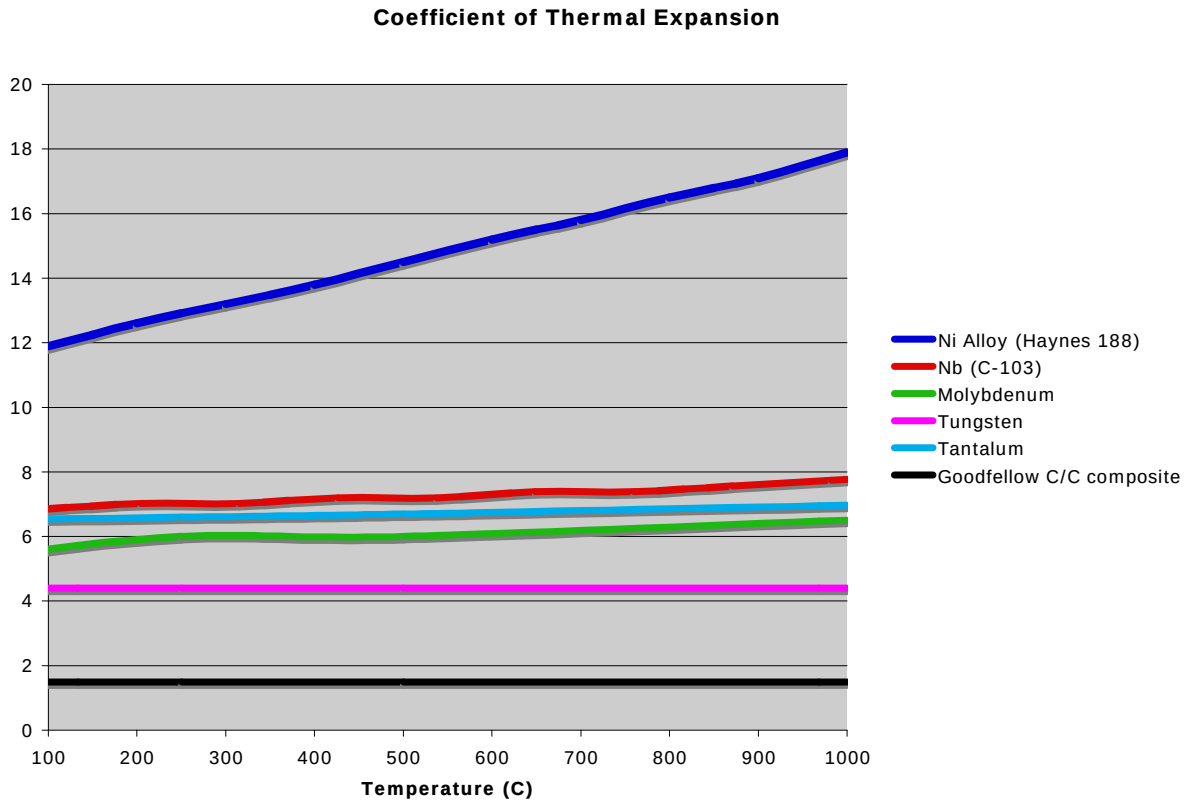

Figure 7: Coefficient of thermal expansion vs. temperature comparison of high temperature materials

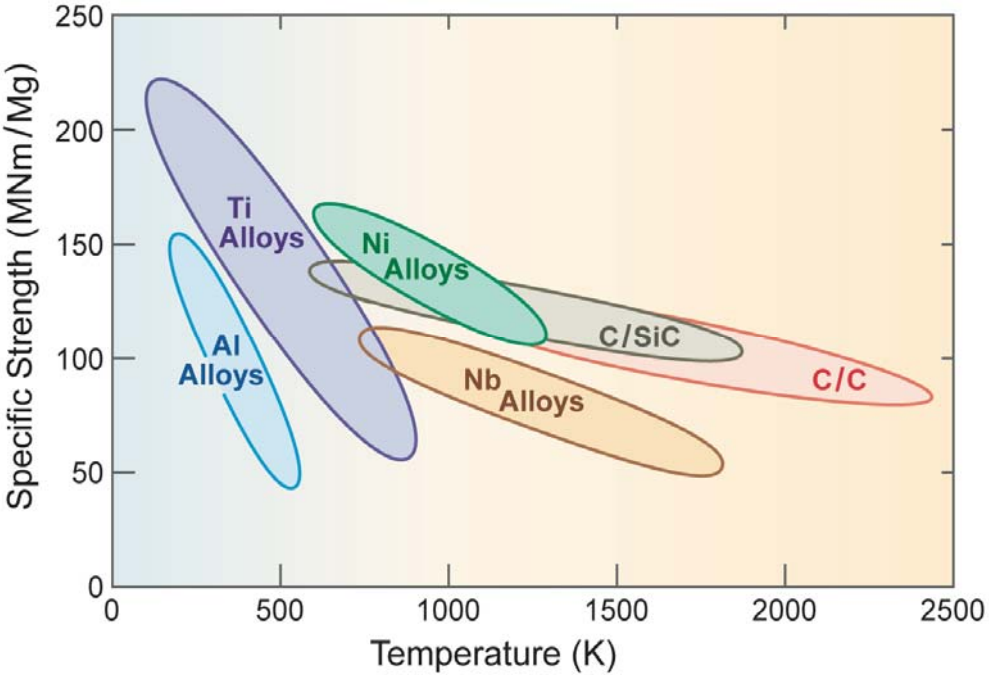

Figure 8: Specific Strength vs. Temperature comparison among several alloy classes [26]

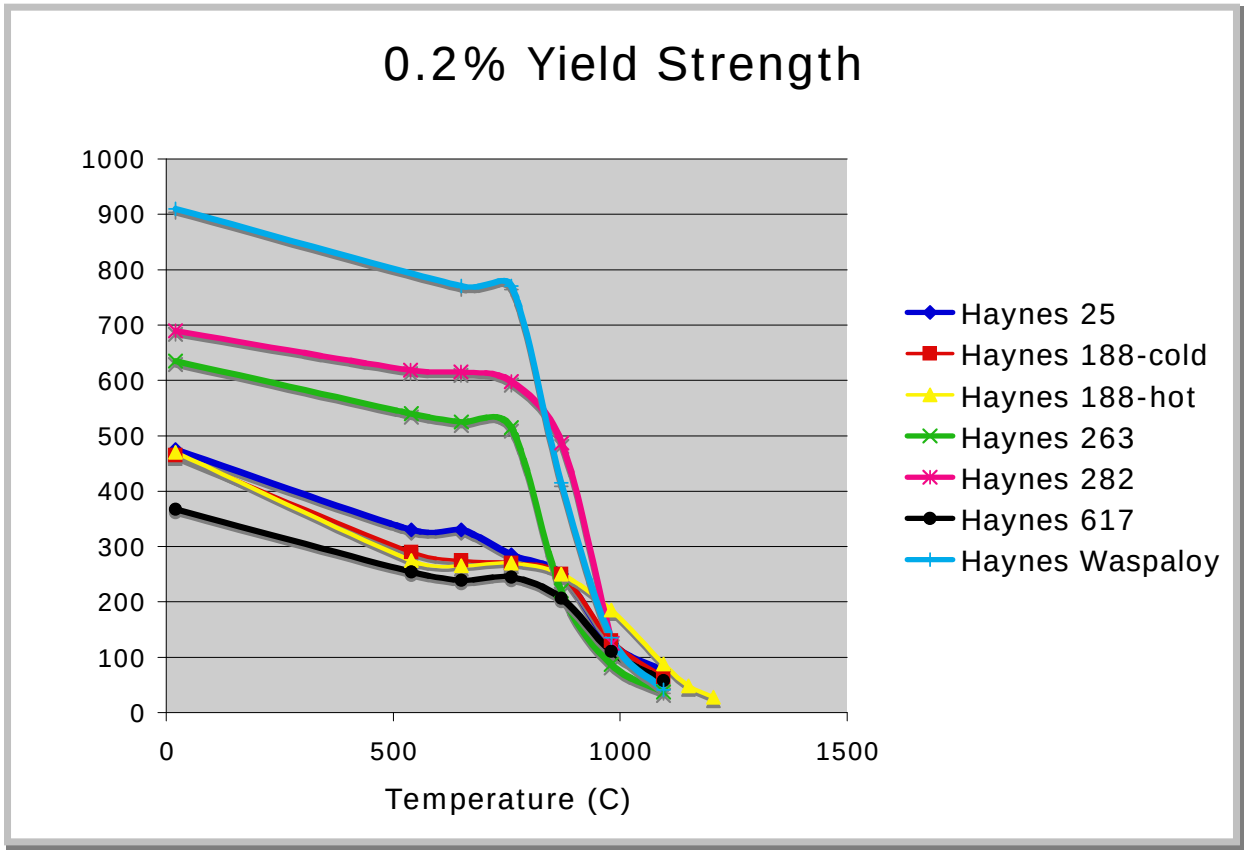

Figure 9: Comparison chart of nickel-cobalt alloys showing yield strength vs. temperature (note: alloy compositions available in Appendix A)

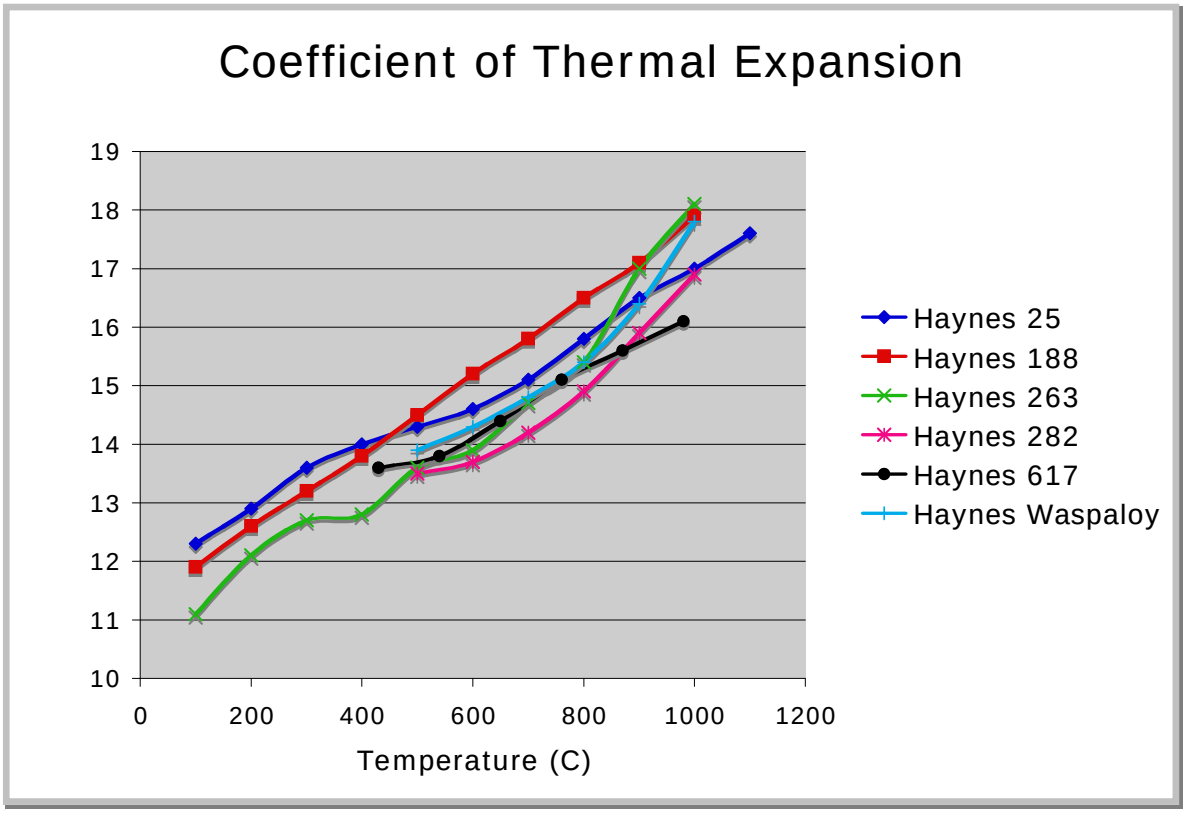

Figure 10: Comparison chart of nickel-cobalt alloys showing coefficient of thermal expansion vs. temperature (note: alloy compositions available in Appendix A)

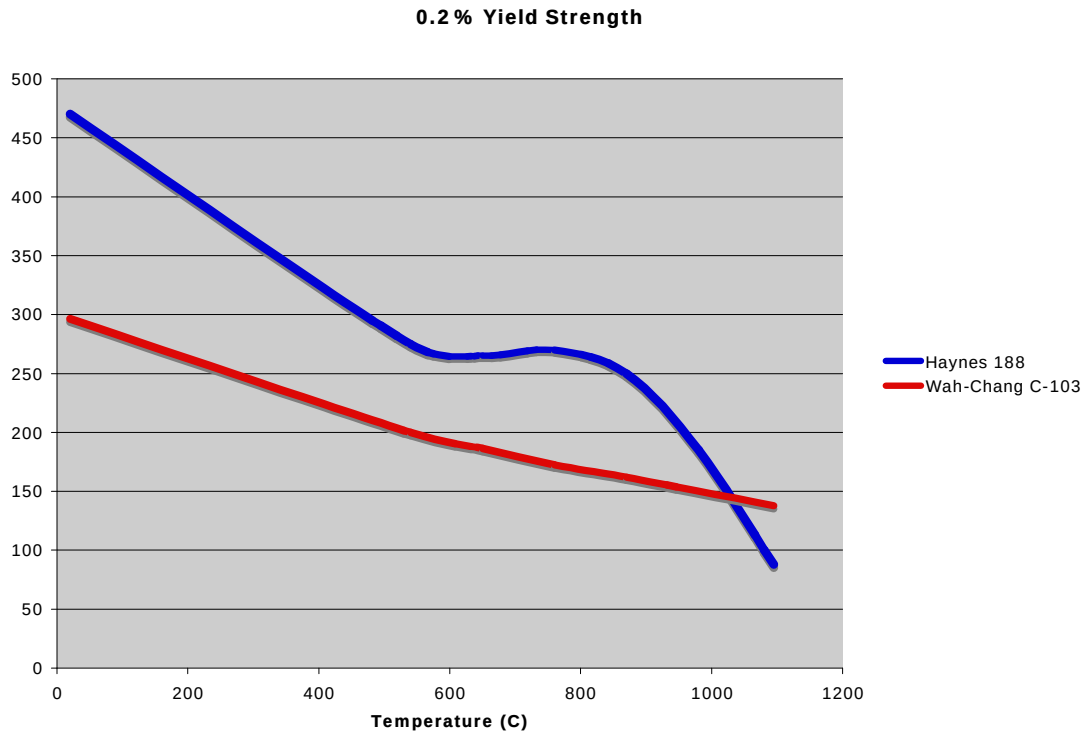

Figure 11: Comparison chart of Haynes 188 and Wah-Chang C-103 showing 0.2% yield strength vs temperature

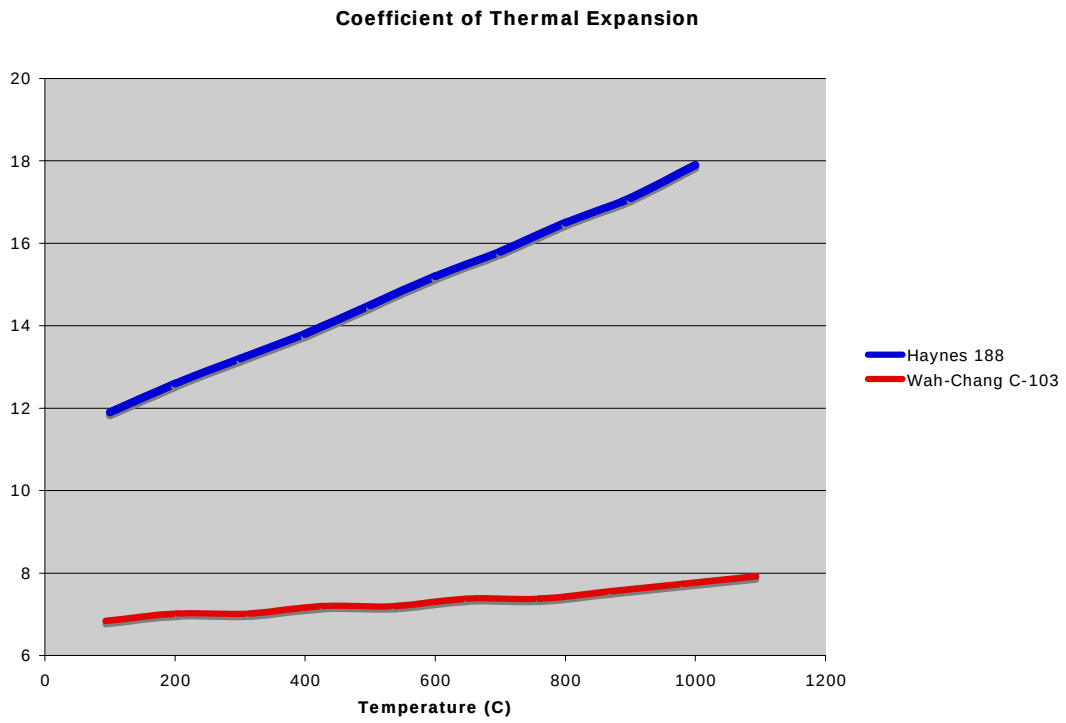

Figure 12: Comparison chart of Haynes 188 and Wah-Chang C-103 showing coefficient of thermal expansion vs. temperature

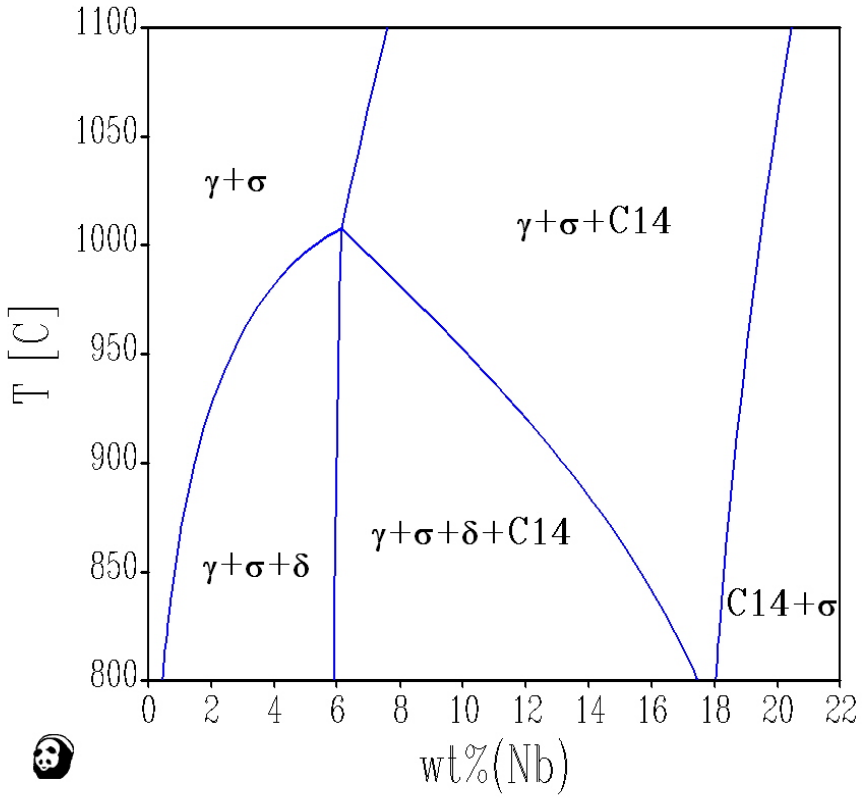

Figure 13: Binary phase diagram of nickel-niobium interdiffusion within Haynes 188

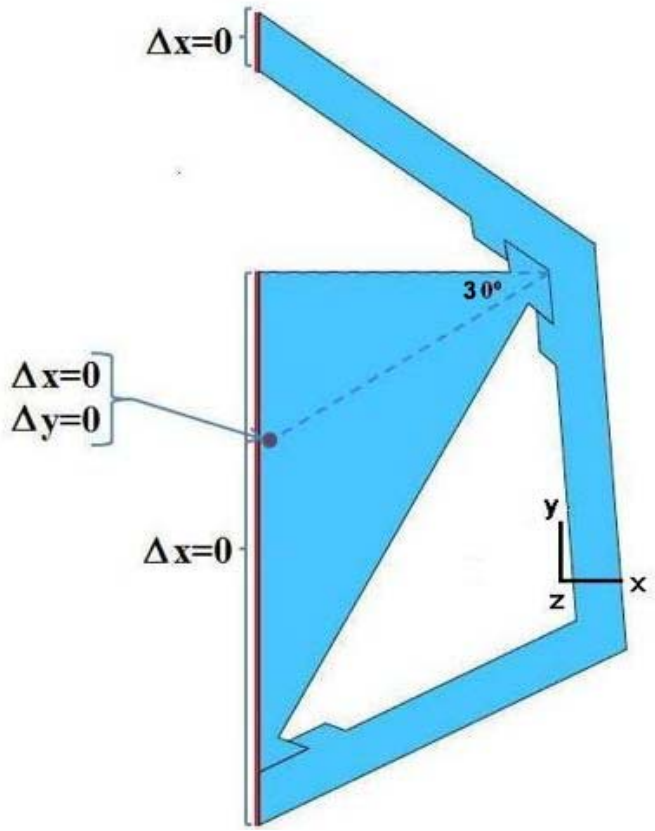

Figure 14: Boundary conditions applied to the lattice model in ABAQUS simulation

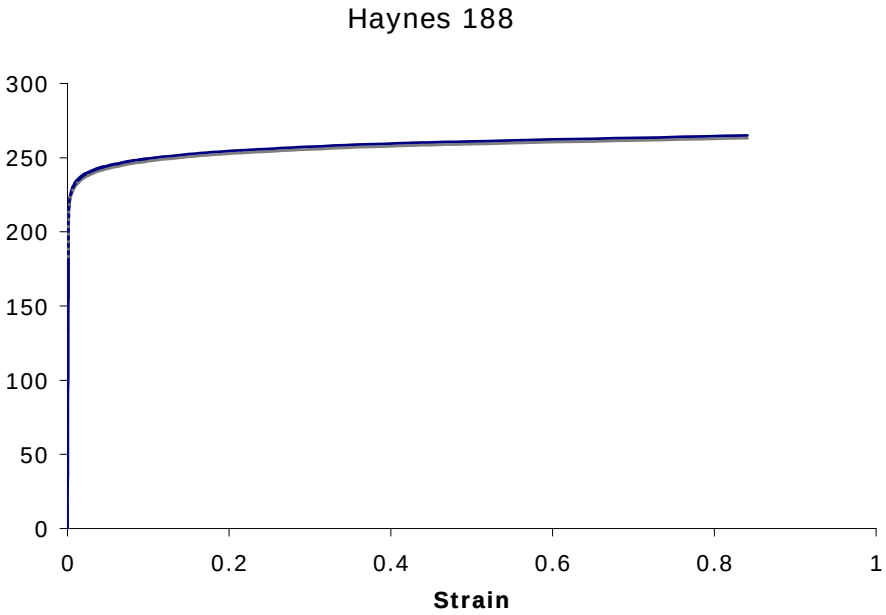

Figure 15: Modeled Stress-strain curves for Haynes 188 at 1000°C.

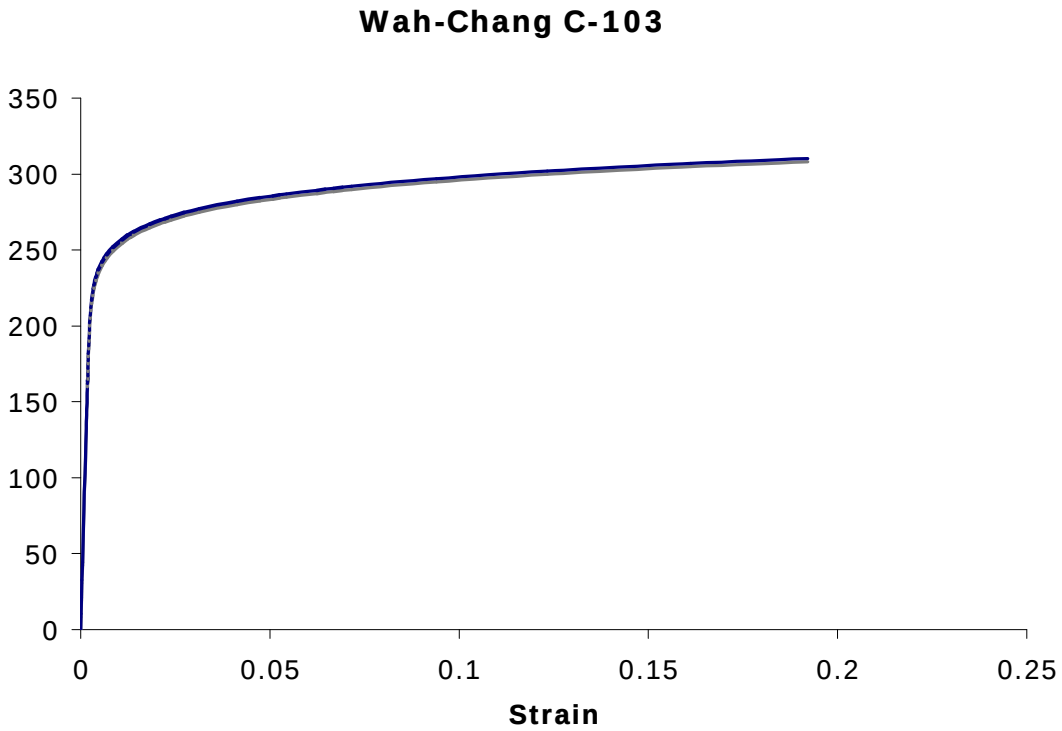

Figure 16: Modeled Stress-strain curve for Wah-Chang C-103 at 1000^{o}C.

Figure 17: Dovetail configuration of lattice cell

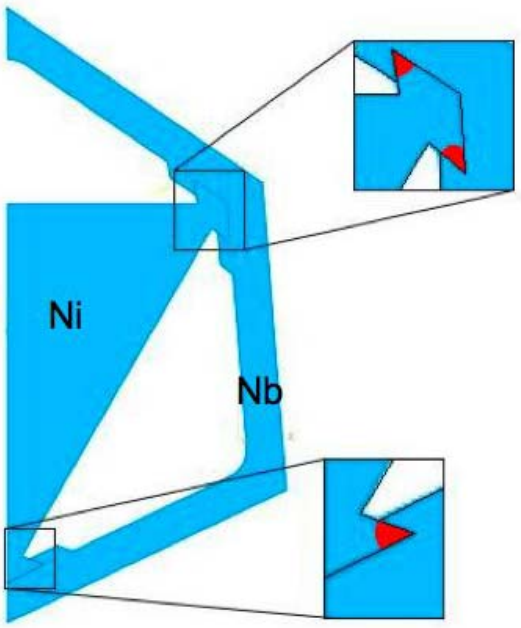

Figure 18: Highest stress concentrations in Haynes 188

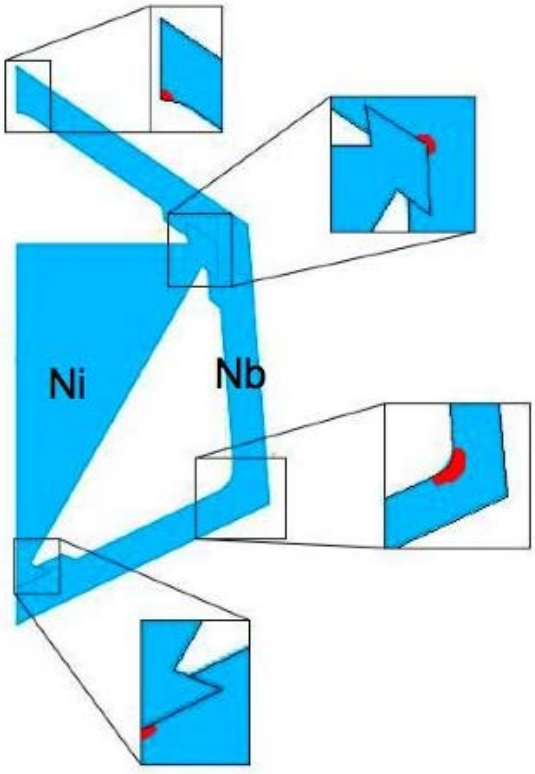

Figure 19: Highest stress concentrations in Wah-Chang C-103

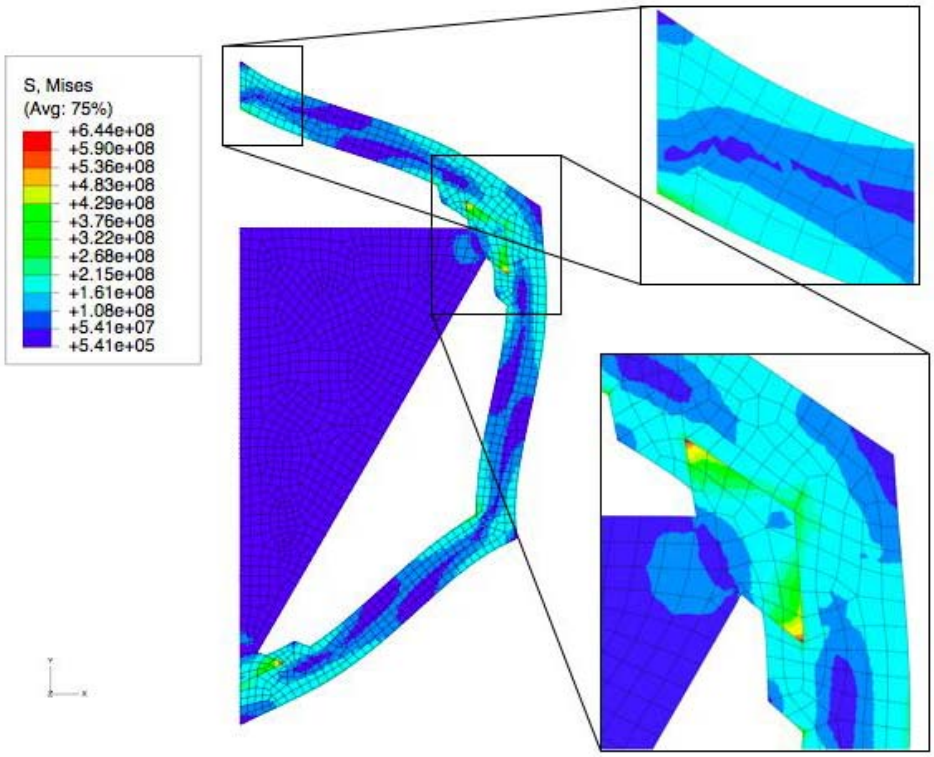

Figure 20: Mises stresses (Pa) in dovetail configuration at 400^{o}C

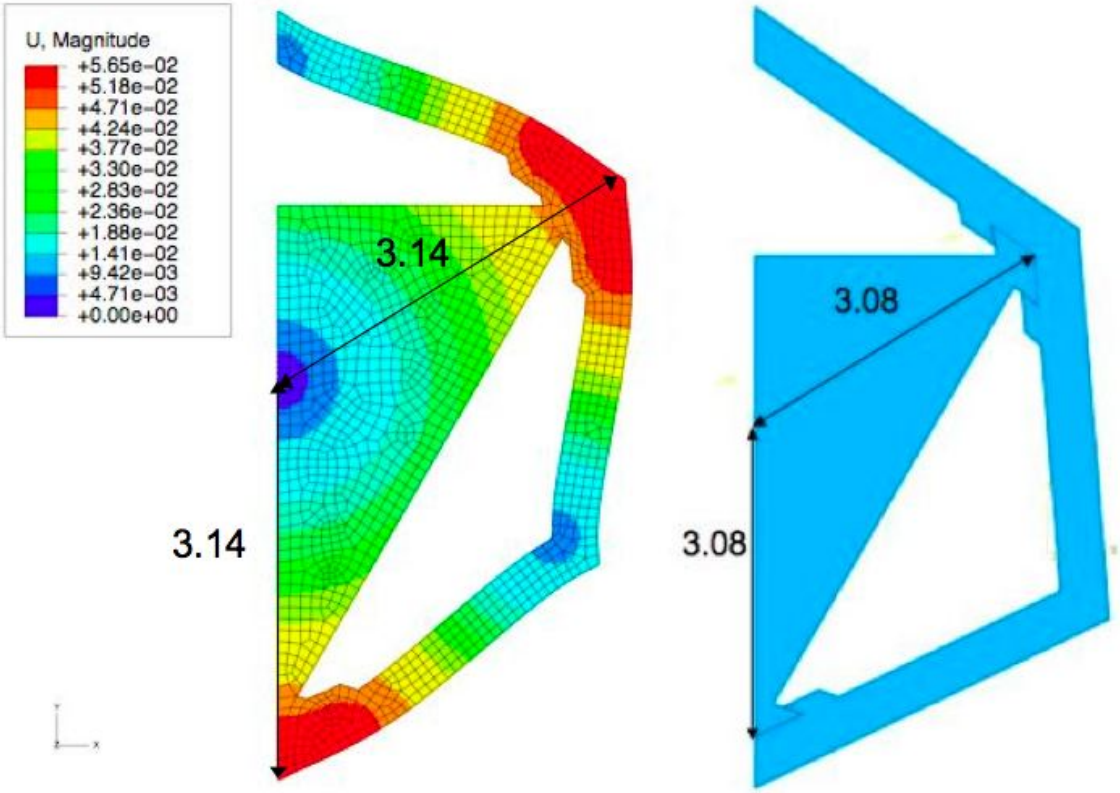

Figure 21: Overall displacement, U, of dovetail configuration at 1000^{o}C

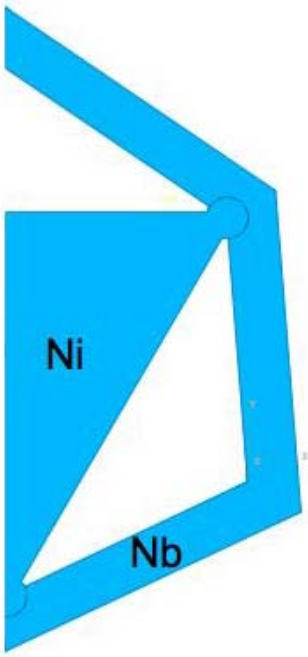

Figure 22: Keyhole configuration of lattice cell

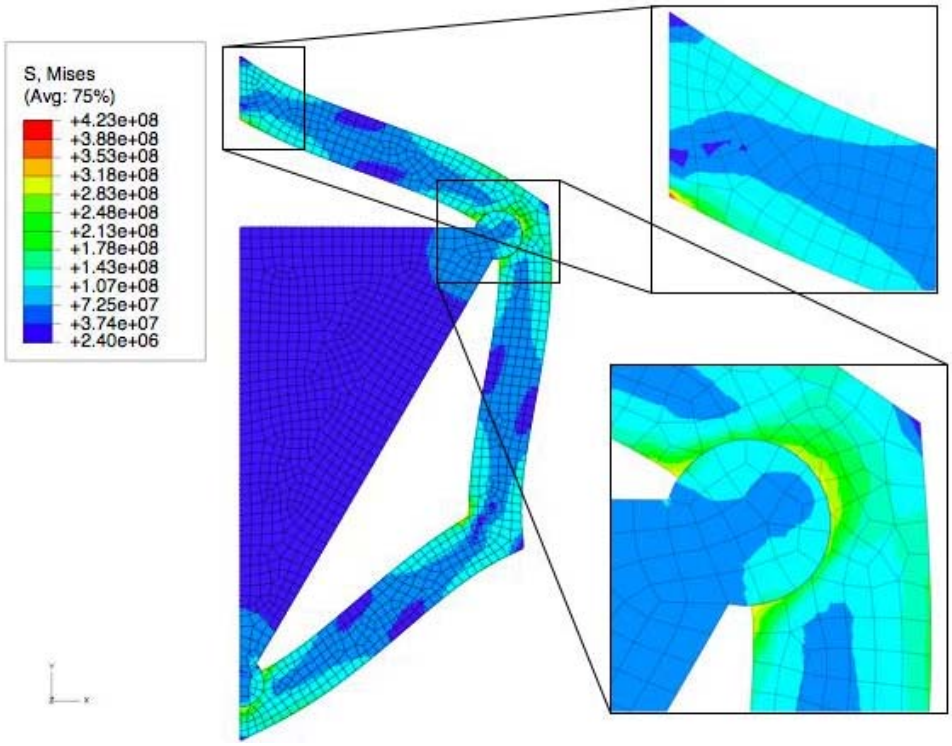

Figure 23: Mises stresses (Pa) in keyhole configuration at 300^{o}C

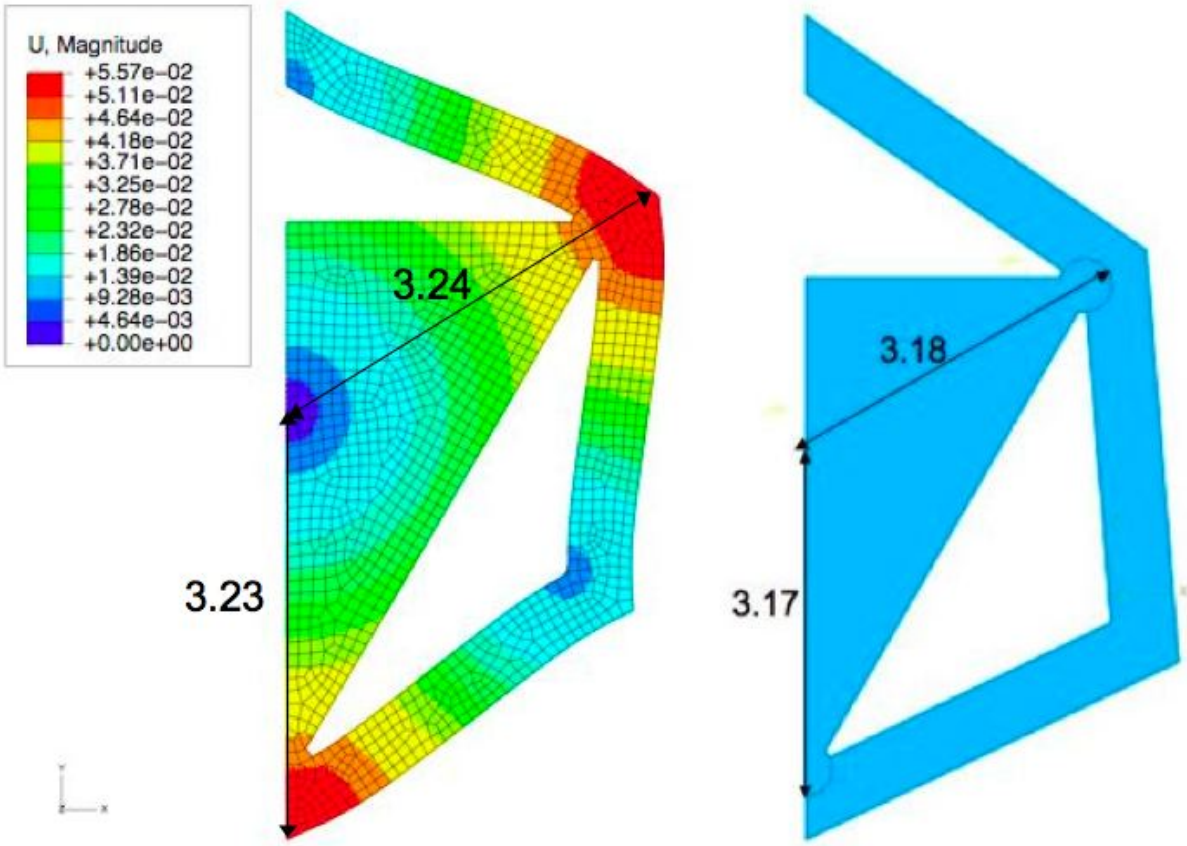

Figure 24: Overall displacement, U, of keyhole configuration at 1000^{o}C

Figure 25: Rounded dovetail configuration

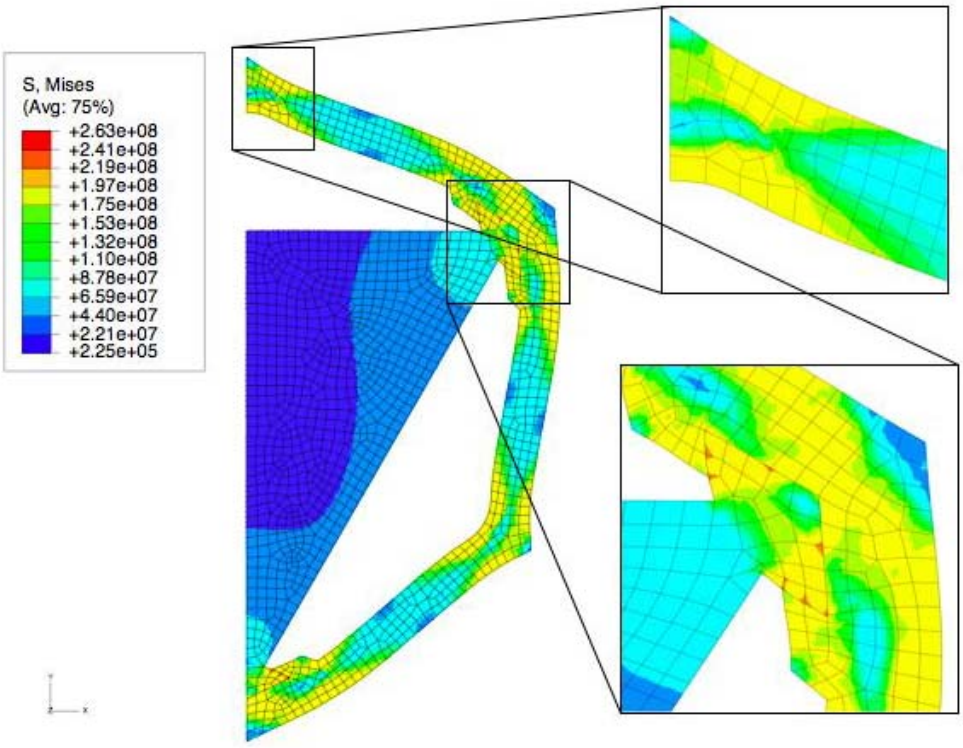

Figure 26: Mises stresses (Pa) for rounded dovetail at 1000^{o}C

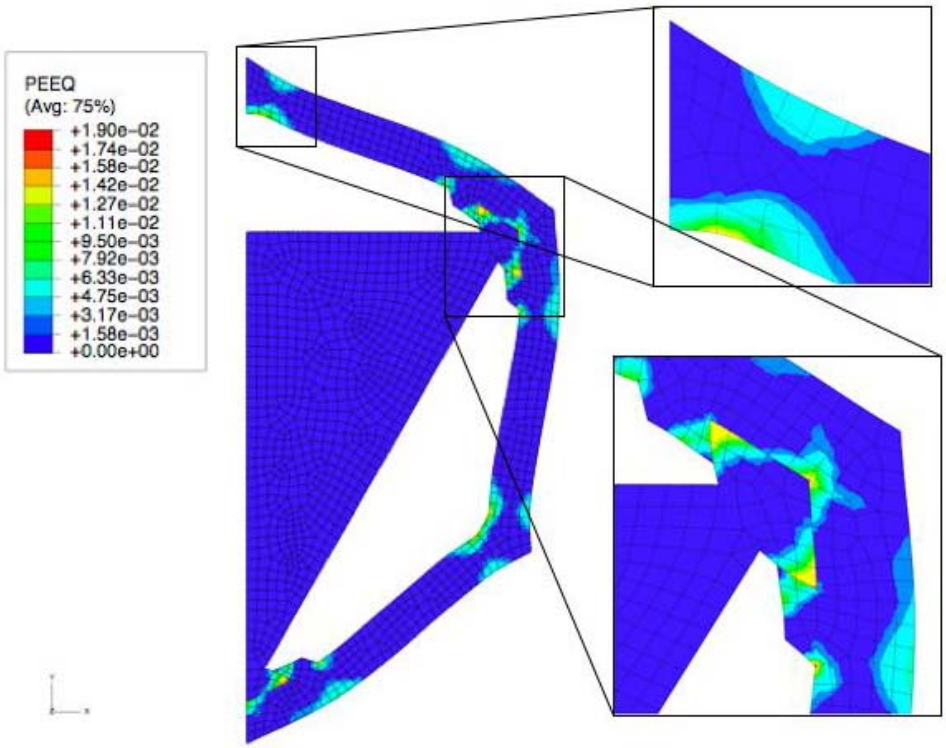

Figure 27: Equivalent plastic strain for rounded dovetail at 1000^{o}C

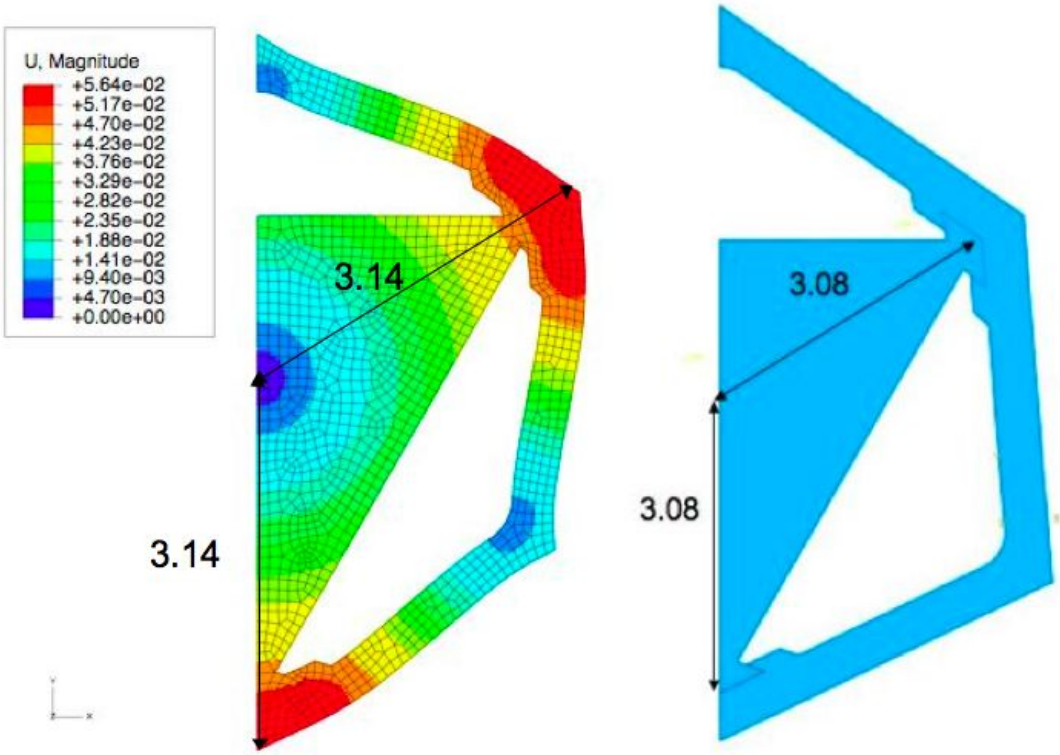

Figure 28: Displacement of rounded dove configuration at 1000^{o}C

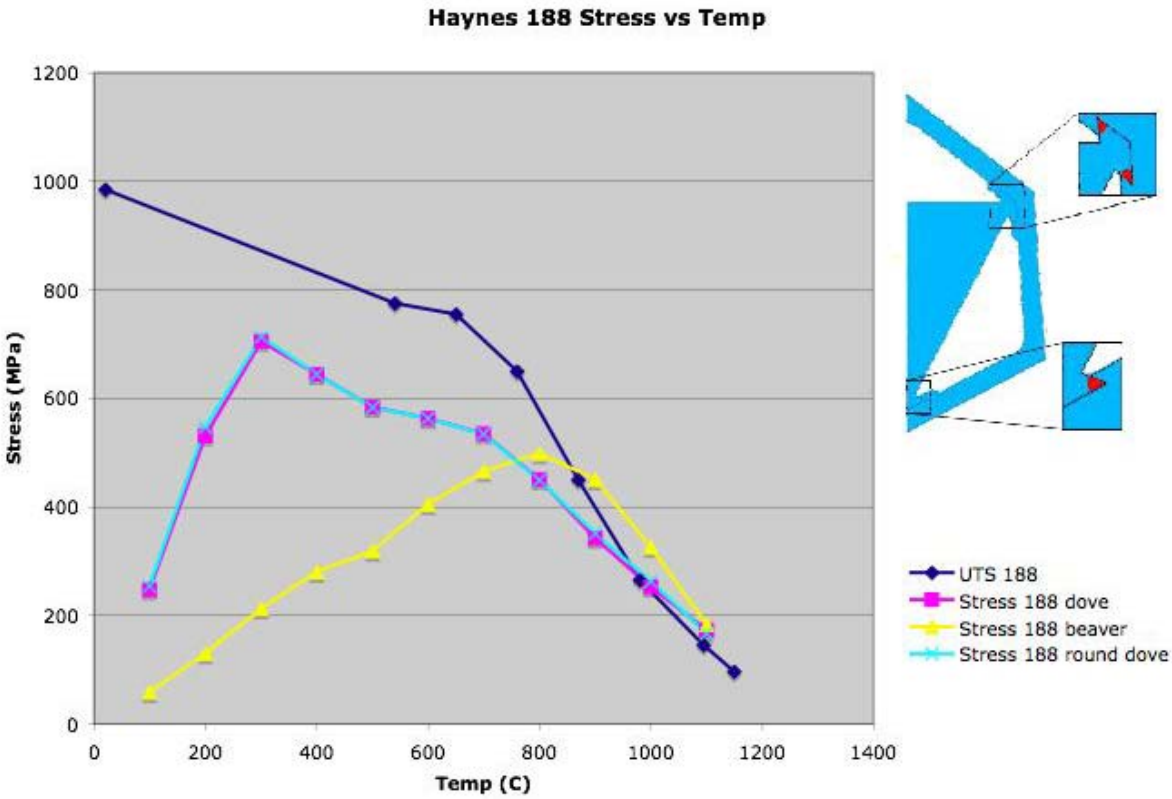

Figure 29: Stress comparison of Haynes 188 for three configurations

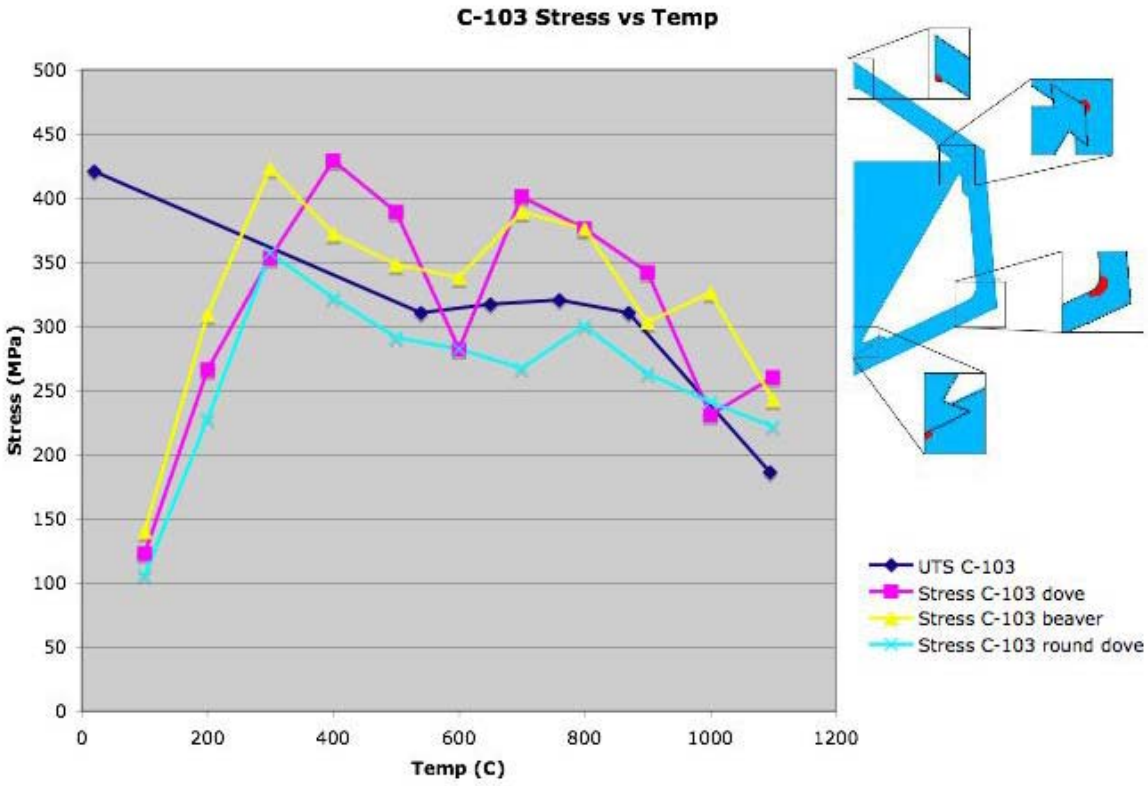

Figure 30: Stress comparison of Wah-Chang C-103 for all three configurations

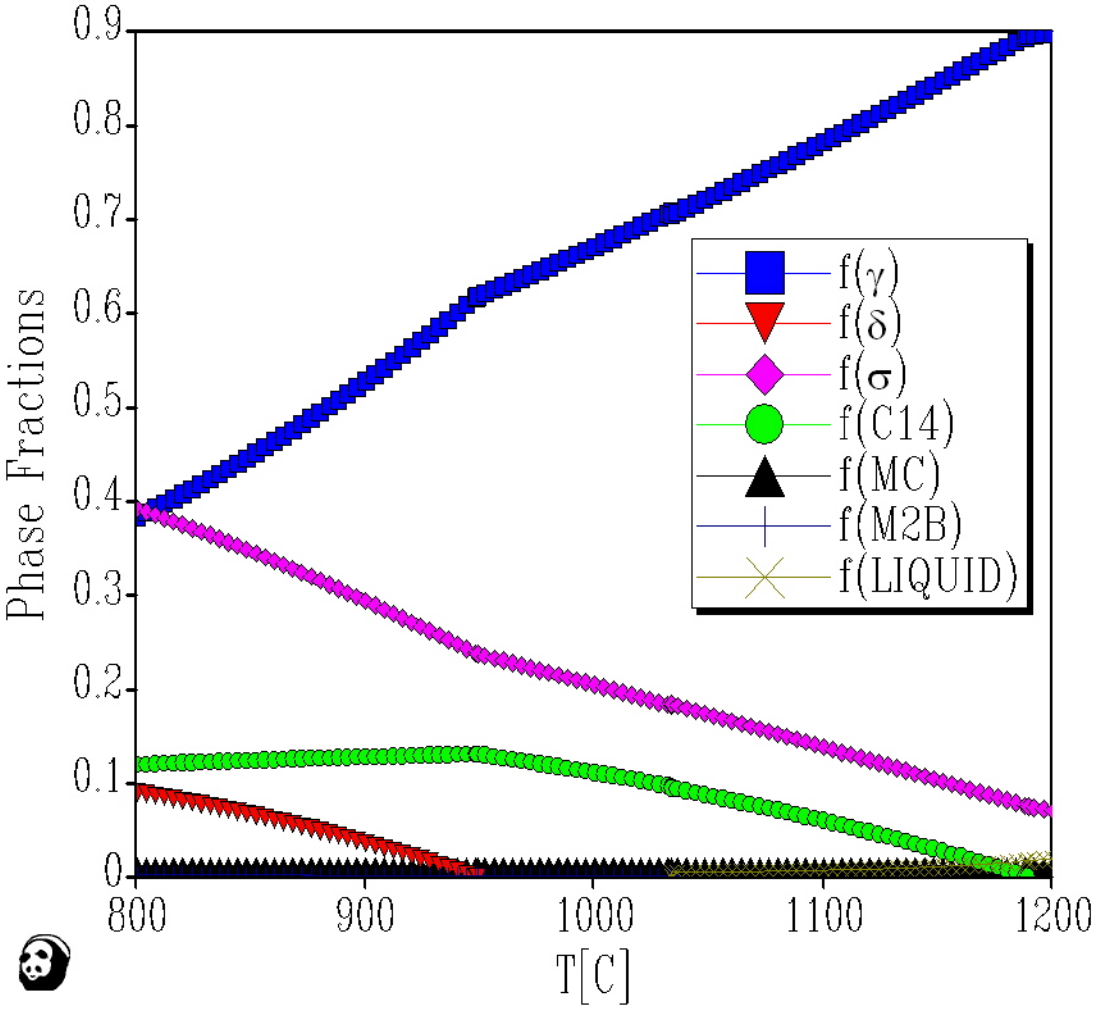

Figure 31: Phase fraction diagram of niobium-nickel interdiffusion within Haynes 188

Appendix A: Nickel-Cobalt alloy comparisons

A comparison on six nickel-cobalt alloys, all manufactured by Haynes International, was done. The chemical composition percentages are given in Table 8 below. The findings indicated that Haynes 188 was the best alloy for this research as it had excellent thermal expansion, elasticity, and strength. Due to its excellent properties as well, Haynes 25 could be used in this experiment; however Haynes 188 is superior.

Table 8: Chemical composition of comparison alloys (wt%)

	Ni	Co	Cr	W	Mo	Ti	Al	Fe
Haynes 25	10	51	20	5	-	-	-	-
Haynes 188	24	38	23	15	-	-	-	-
Haynes 263	52	20	20	-	6	-	-	-
Haynes 282	57	10	19.5	-	8.5	2.1	1.5	1.5
Haynes 617	54	12.5	22	-	9	-	1.2	1
Haynes waspalloy	58	13.5	19	-	4.3	3	1.5	2

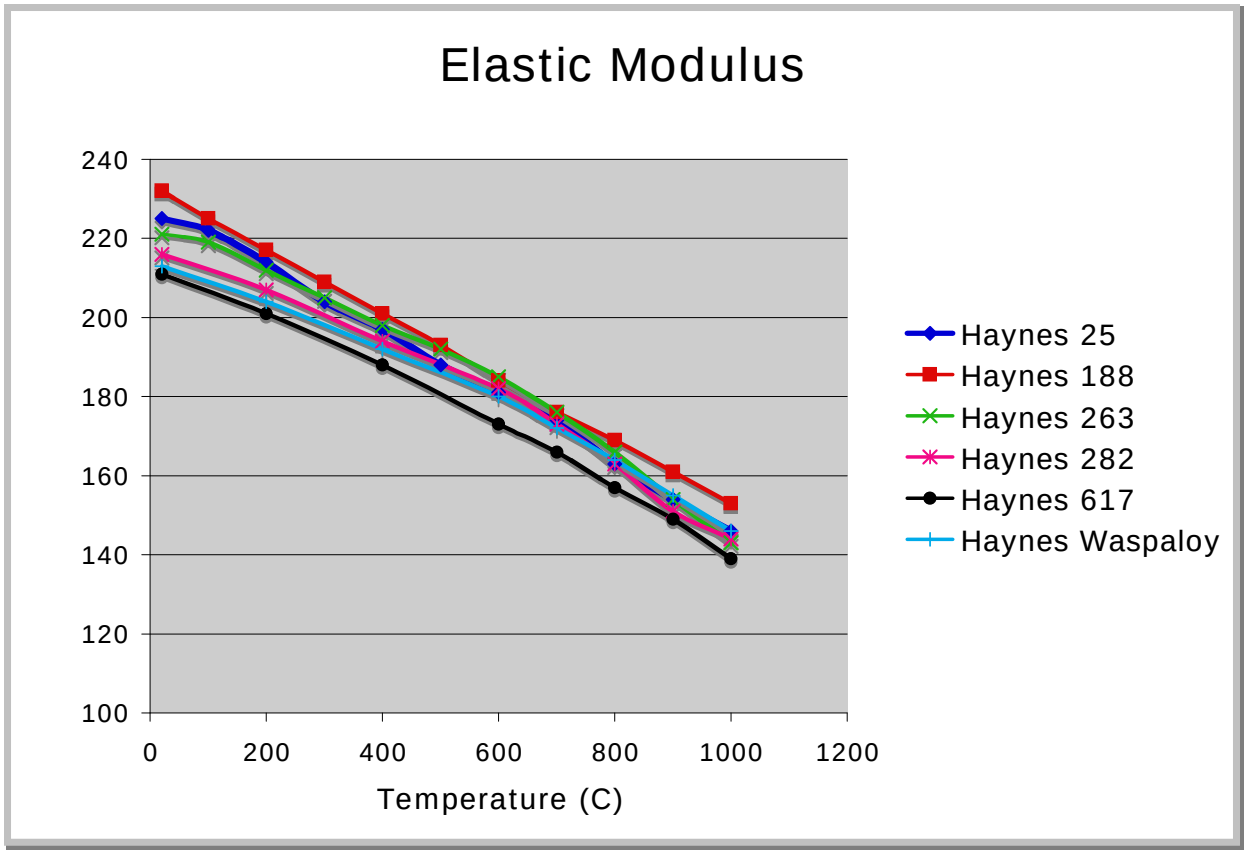

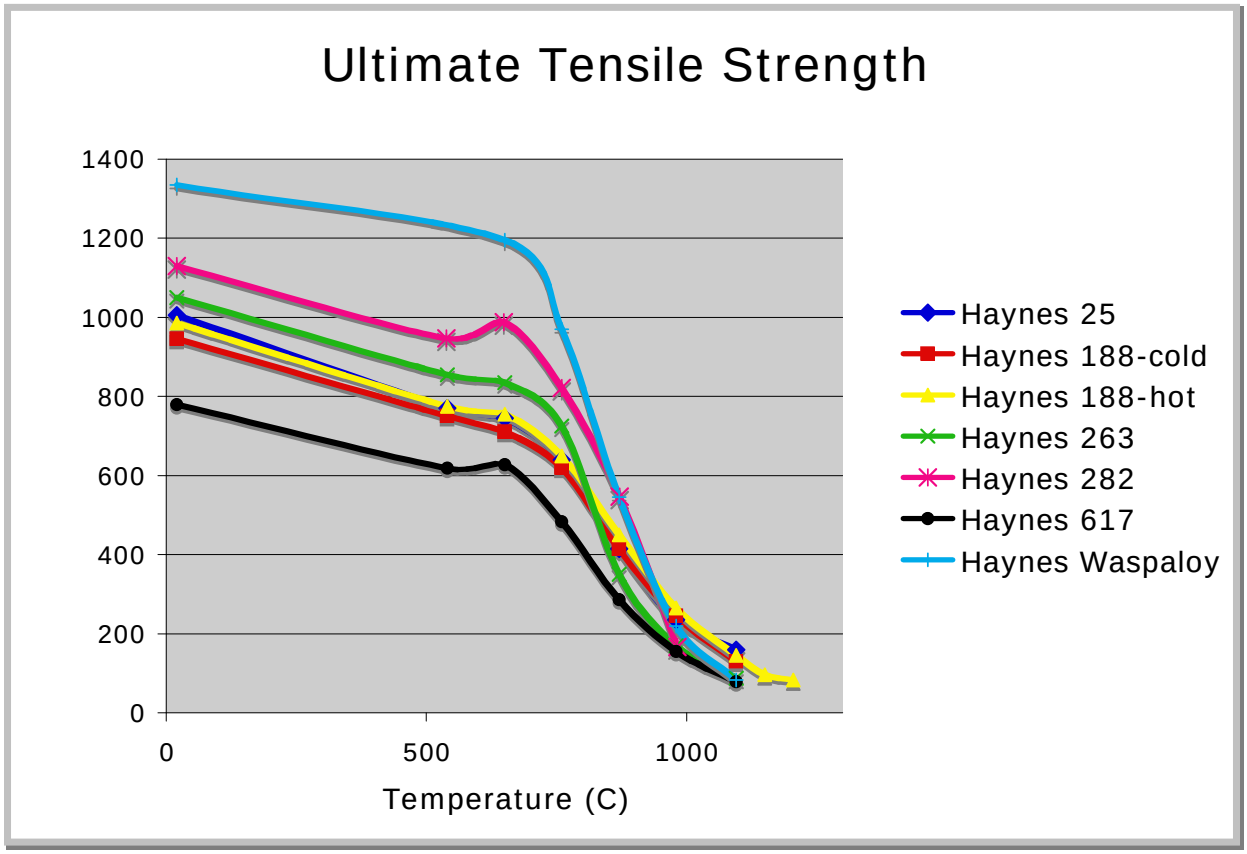
Ultimate Tensile Strength
1400
1200
1000
800
600
400
200
0
0
500
1000
Temperature (C)
Haynes 25
Haynes 188-cold
Haynes 188-hot
Haynes 263
Haynes 282
Haynes 617
Haynes Waspaloy